

Scientific paper

A Facile Route to the Synthesis of Coated Maghemite Nanocomposites for Hyperthermia Applications

Gregor Ferk,¹ Irena Ban,^{1,6,*} Janja Stergar,¹ Darko Makovec,²
Anton Hamler,³ Zvonko Jagličič^{4,5} and Miha Drofenik^{1,2}

¹ University of Maribor, Faculty of Chemistry and Chemical Engineering, Smetanova 17, SI-2000 Maribor, Slovenia

² Jožef Stefan Institute, Department for Materials Synthesis, Jamova 39, SI-1000 Ljubljana, Slovenia

³ University of Maribor, Faculty of Electrical Engineering and Computer Science, Smetanova 17, SI-2000 Maribor, Slovenia

⁴ Institute of Mathematics, Physics and Mechanics, Jadranska 19, SI-1000 Ljubljana, Slovenia

⁵ University of Ljubljana, Faculty of Civil and Geodetic Engineering, Jamova 2, SI-1000 Ljubljana, Slovenia

⁶ Center of Excellence NAMASTE, Jamova 39, SI-1000, Ljubljana, Slovenia

* Corresponding author: E-mail: irena.ban@uni-mb.si

Tel: +386 2 2294 417; Fax: +386 2 2527 774

Received: 06-01-2012

Abstract

CM-dextran-covered maghemite particles for applications in magnetic hyperthermia treatments were synthesized and their physical, magnetic and morphological properties were examined. Magnetic fluids were prepared and their heating properties in an alternating magnetic field were studied. The results reveal that the particle size and the thickness of the carboxy-methyl-dextran (CM-dextran) coatings have a decisive influence on the heating properties: specific absorption rate (SAR). The majority of the magnetic dissipation comes from the Neel relaxation, while the Brown contribution is small. A thermal steady state at the selected temperature (42 °C) can be achieved using synthesized maghemite particles with proper particle morphology and by controlling the magnetic field intensity or the frequency.

Keywords: Magnetite nanoparticles, hyperthermia, magnetic properties.

1. Introduction

Magnetic nanoparticles and their derivatives, magnetic fluids, are being investigated for various applications, including resonance imaging,¹ drug delivery,² magnetic separation³ and magnetic hyperthermia.^{4,5}

The magnetic nanoparticles and/or their derivatives normally consist of polymer-covered ferrimagnetic iron oxides, which are synthesized in situ by precipitation in the presence of polymers that act as a stabilizer. It has been noted that materials based on precipitated ferrimagnetic iron oxides generally give superior results, compared with other types of magnetic materials. In addition, precipitated iron oxides were shown to produce little, if any, toxicity to humans. This means that iron oxides are,

because of their high magnetization, biocompatibility, simple synthesis and a relatively high magnetic dissipation, among the most attractive materials, with the only weakness being that they possess a relatively high Curie point that may cause the tissue to overheat. However, the generated heat can be effectively controlled by selection of the particle morphology⁶ and the alternating magnetic field (AMF) intensity and/or frequency.⁷ When we are able to control all these parameters and reach thermal equilibrium in such a way that the generated heat at the selected temperature and location will be equal to that lost to the environment due to the thermal convection or heat exchange to the veins, no overheating of the surrounding tissue will take place. In this case iron oxide can still be used, in spite of its high transition temperature. For this

reason it is of crucial importance to be able to precisely determine the specific absorption rate (SAR) of the magnetic energy absorbed by the magnetic particles dispersed in the magnetic fluid (MF). This magnetic energy is then transformed into the heat that warms up the MF under consideration.

A variety of nanocomposites (polymer-coated magnetic particles) dispersed in water have been prepared in the past, for example, water-soluble dextran,⁸ polyvinyl alcohol,⁹ poly(ethylene glycol),¹⁰ amylose starch¹¹ and chitosan biopolymer.¹² Among them, CM-dextran is a polysaccharide with outstanding properties, as well as being biodegradable, biocompatible and bioactive, and as such is commonly used for the stabilization of MFs.¹³

In this work we synthesized MFs using maghemite particles with a proper morphology stabilized by CM-dextran. We achieved a steady state at the selected temperature using synthesized maghemite particles with a proper particle morphology and by applying a controlled magnetic power.

2. Experimental

2.1. Reagents and Materials

For the synthesis of the maghemite particles coated with CM-dextran the following chemicals were used: $\text{FeCl}_2 \cdot 4\text{H}_2\text{O}$ and $\text{FeCl}_3 \cdot 6\text{H}_2\text{O}$ (Acros Organics), sodium carboxymethyl – dextran salt (CM-dextran; Fluka Biochemika with $M = 14400$ g/mol), Tryptic Soy Agar (Fluka) and 25% NH_4OH (Alkaloid Skopje). During the synthesis of the magnetic fluid, ultrasound radiation was applied with an ultrasonic generator (Sonics Vibra Cell 750 W intensity).

2.2. Synthesis

The detailed procedure for sample A was as follows:

A total of 125 mL of a solution containing Fe^{2+} (0.135 mol/L) and Fe^{3+} (0.113 mol/L) ions was poured into a 250-mL beaker equipped with a magnetic stirrer and then heated to 80 °C. When a temperature of 80 °C was achieved, 50 mL of 25% NH_4OH was added (pH > 9). The solution turned from a red-brown color to black, indicating the formation of magnetite, which then oxidized to maghemite. The suspension was then aged at 80 °C for 1 hour and cooled to room temperature. The suspension was magnetically decanted and the magnetic particles were washed several times with distilled water.

The detailed procedure for sample B was as follows:

The same as sample A, but immediately after the addition of NH_4OH , 10 ml of the CM-dextran solution (10 g CM-dextran / 20 g H_2O) was added in several successive small additions over a period of 30 minutes. The suspen-

sion was then aged at 80 °C for 30 minutes and cooled to room temperature. The suspension was magnetically decanted and the magnetic particles were washed several times with distilled water. To the magnetically decanted particles, 10 mL of CM-dextran solution was added and sonicated for 1 hour to obtain the magnetic fluid (MF). In order to sediment the agglomerates, the MF was centrifuged at 5000 rpm for 5 min and the supernatant was ultrafiltrated with a UF membrane $Mw_{\text{cut-off}} = 100$ kDa to produce a MF with a large content of iron oxide particles. For the SAR measurement we prepared a MF with 9.75% (wt) of iron oxide.

For the SAR measurements in agar:

Agar was added to the MF with a high content of iron oxide particles and during stirring heated to 70 °C to obtain a very viscous fluid. After that the content was poured into the measuring cuvette and cooled to room temperature, after which a hard gel was obtained. The content of iron oxide in the gel was 9.75% (wt).

2.3. Analysis and Measurements

The nanoparticles were characterized using X-ray diffraction analyses (Bruker Axs, D 5005) and a transmission electron microscope (TEM) (JEOL 2010F). The particle size was established using the Scherrer method, based on the broadening of the X-ray diffraction peaks. The particle size and the size distribution were determined from the TEM images. Dynamic light scattering (Horiba LB-550) was used to estimate the CM-dextran-maghemite hydrodynamical size distribution (d_H).

The presence of the CM-dextran was confirmed by FTIR spectroscopy (PERKIN ELMER 1600), while the amount/concentration of CM-dextran adsorbed onto the magnetic particles was determined by a thermogravimetric analysis (TGA) (TGA/SDTA 851, Mettler Toledo). The magnetization was measured with a helium-cooled superconducting quantum interference device (Quantum Design MPMS-XL-5 SQUID magnetometer).

In our investigation a conventionally built system was used to generate an alternating magnetic field with a nominal field strength of 2 kA/m and a maximum frequency of 104 kHz. For the calorimetric measurements of the magnetic fluid losses a sample of magnetic fluid was placed in a glass vial in the center of the surrounding supply coil. The length of the coil was twice the length of the glass vial in order to guarantee a homogeneous field in the center of the vial. The glass vial was placed in some heat-insulating polystyrene to reduce the heat dissipation from the magnetic fluid to the surroundings and vice versa. The thermal measurements were performed using a fiber-optic thermometer in the presence of the magnetic field. The calorimetric measurements were carried out using a calorimeter, where the heat effects can be determined by an im-

mediate measurement of the temperature. In that case the calorimeter is a measurement system and the heat effects are due to the absorption of magnetic energy when subjected to an alternating magnetic field. The measurements were continued until a steady state is achieved, i.e., until the heat induced equals the heat dissipated. For more see ref..¹⁴

3. Results and Discussion

3. 1. X-ray Diffraction Analysis

Fig. 1 shows the X-ray diffraction patterns of the as-prepared maghemite particles (A) and the particles covered with CM-dextran (B). All the diffraction peaks displayed by the diffractogram correspond to the maghemite cubic phase (JCPDS No.39-1346). From the X-ray line broadening and the Sherrer formula it is possible to estimate an average particle size of 16.0 nm for sample (A) and 11.8 nm for sample (B).

Typical TEM images of the as-synthesized sample (A) and the CM-dextran-coated maghemite nanoparticles (B) are shown in Figs. 2a and 2b, and the corresponding grain-size distributions obtained from the TEM images

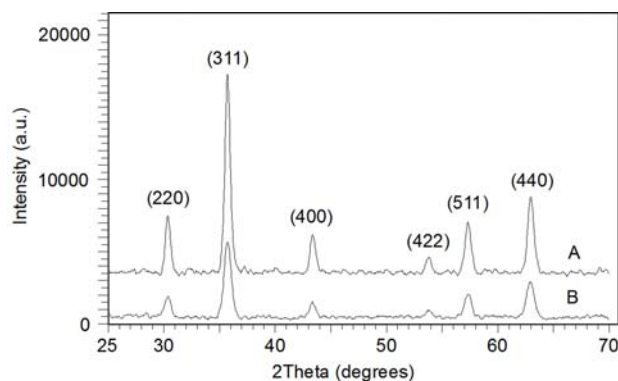


Fig. 1. XRD spectra of as-prepared samples (A) and of maghemite particles covered with CM-dextran (B).

are shown in Figs. 2c and 2d. The average particle diameters estimated from the TEM images are 14.5 nm for sample (A) and 12.0 nm in sample (B), in good agreement with X-ray diffraction analysis. The main reason that the coated particles showed a smaller average particle size is because they were centrifuged, which eliminates the larger particles from the MF.

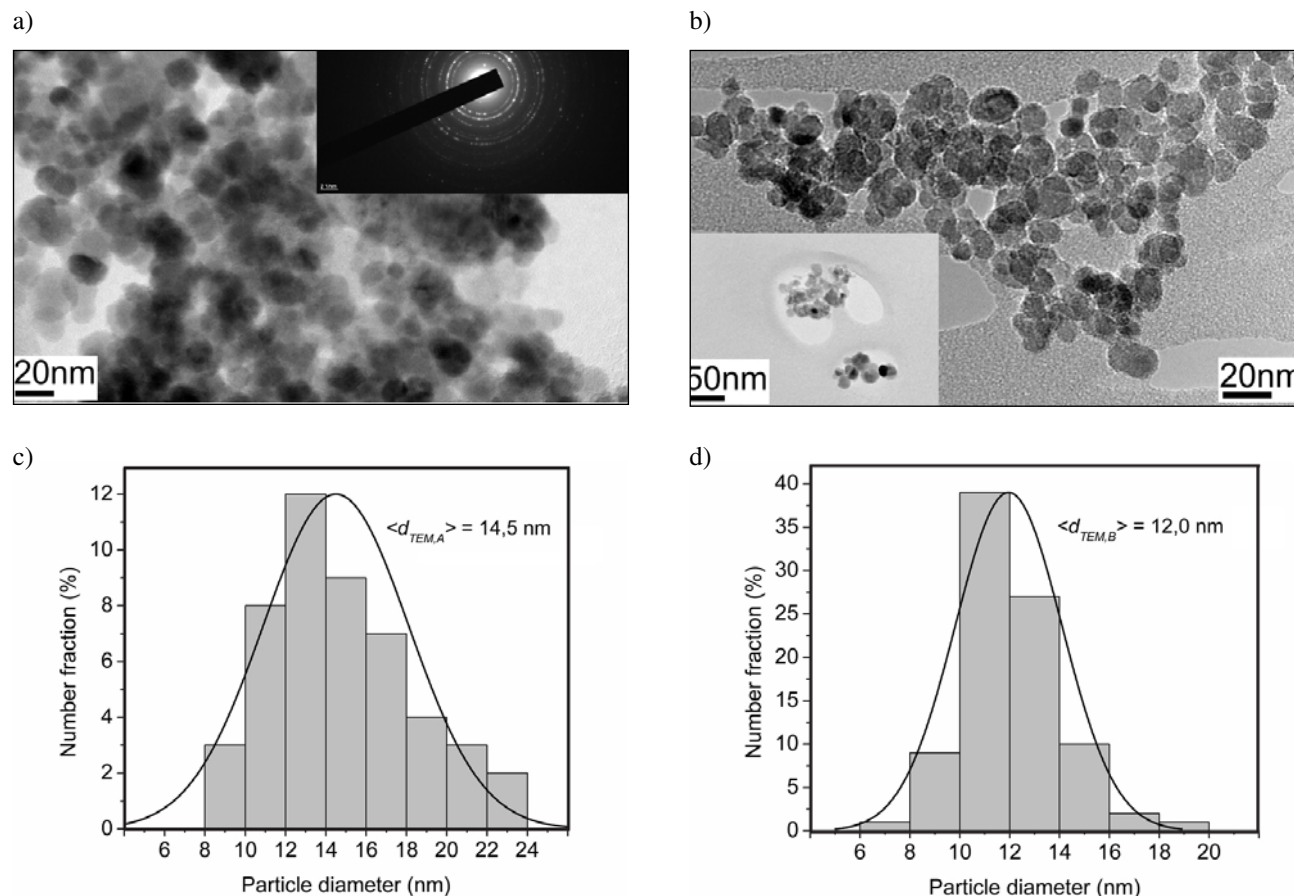


Fig. 2. TEM images of a) as-synthesized maghemite particles (A), b) CM-dextran-stabilized maghemite particles (B)-insert; smaller agglomerates, c) the grain size distribution of the uncoated particles (A) and d) the CM-dextran-coated particles (B).

3. 2. TGA and SDTA Analysis

The distinctive weight losses established for the magnetic particles covered with CM-dextran can be divided into two temperature regions: 150–500 °C and 500–750 °C, Fig. 3. A total weight loss of 21.2% (sample B) occurred during the thermal heating from room temperature to 750 °C. In the first temperature range, from 150 °C to 500 °C, the oxidation of the CM-dextran occurs, as indicated by an exothermic simultaneous differential thermal analysis (SDTA) peak and a weight loss of 16.4%. The exothermic peak associated with this mass loss is the result of the oxidation of the CM-dextran molecules due to the temperature, which is consistent with the literature data on free polysaccharides at 230–400 °C.¹⁵ The last step is associated with a weight loss of 3.1%, which is associated with the removal of the CM-dextran covalently bound to the particle surface, i.e., the very first covalent bound layer of CM-dextran to the particle surface.

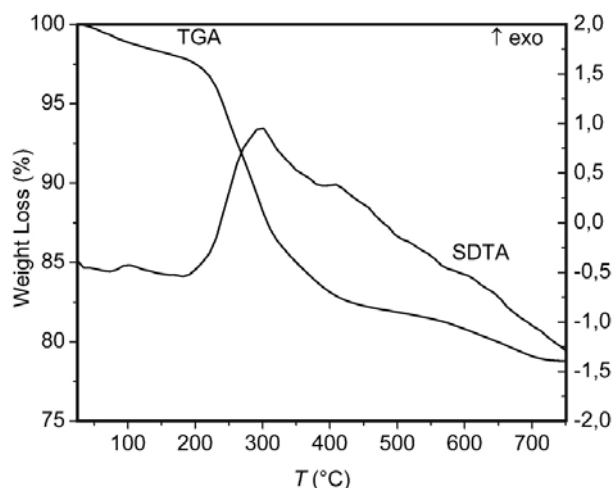


Fig. 3. Thermal analysis (TGA) of the maghemite nanoparticles coated with CM-dextran and the corresponding SDTA.

It is well known that CM-dextran dissolved in water is in equilibrium with that attached physically to the magnetic particles. Namely, after the very first layer of CM-dextran, which is covalently bound to the particle surface, the subsequent layers are attached by physical bonds, where hydrogen bonding prevails. In the water suspension this dextran is in equilibrium with the dextran in the suspension.¹⁶

3. 3. Fourier Transform Infrared Spectroscopy (FTIR) and Dynamic Light Scattering Analysis (DLS)

The CM-dextran coatings were investigated using FTIR spectroscopy. In Fig. 4 the FTIR spectra of the mag-

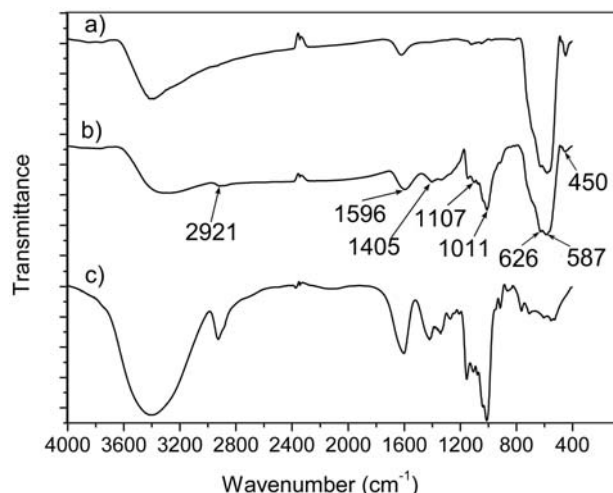


Fig. 4. FTIR spectrum of a) maghemite particles b) maghemite particles coated with CM-dextran and c) CM-dextran.

hemite nanoparticles a), maghemite nanoparticles coated with CM-dextran b) and pure CM-dextran c) are shown.

The absorption bands at 450 cm^{-1} , 587 cm^{-1} and 626 cm^{-1} in the FTIR spectra of iron oxide nanoparticles with and without a CM-dextran coating are attributed to the multiple lattice absorption bands of partially ordered maghemite.¹⁷ The broad band in the region between 3200–3600 cm^{-1} is assigned to O-H stretching. The absorption band at 1596 cm^{-1} is attributed to asymmetric COO stretching in alkali carboxylic acid salts,¹⁸ which indicated the existence of free alkali carboxylate groups on the nanoparticles surface. The observed symmetrical C=O stretching at 1404 cm^{-1} suggested that the carboxylate was bound symmetrically to the surface of nanoparticles, as one of the possible carboxylate binding modes.¹⁹ Moreover, adsorption bands at 2921 cm^{-1} (C-H stretching), 1107 cm^{-1} (C-O-C stretching) and characteristic peak of CM-dextran at 1011 cm^{-1} additionally supports the attachment of CM-dextran onto the maghemite nanoparticles surface.

Hydrodynamic diameter and particle size distribution of the CM-dextran-coated maghemite nanoparticles was inspected with measuring the DLS. From the Fig 5 hydrodynamic diameter d_H was found to be approximately 77.9 nm with the broad size distribution.

3. 4. Magnetic Properties

The zero field cooling (ZFC) and field cooling (FC) curves in Fig. 6a indicate that the particles in sample (B) are superparamagnetic and show a broad maximum at around 200 K, shifted with respect to the point where the ZFC and FC curves coincide. This is an indication of the particle agglomeration and the spread of the particle size. In this case a unique K using the relation $T_B = VK/25k_B$ for the assembly of the particles in sample (B) cannot be

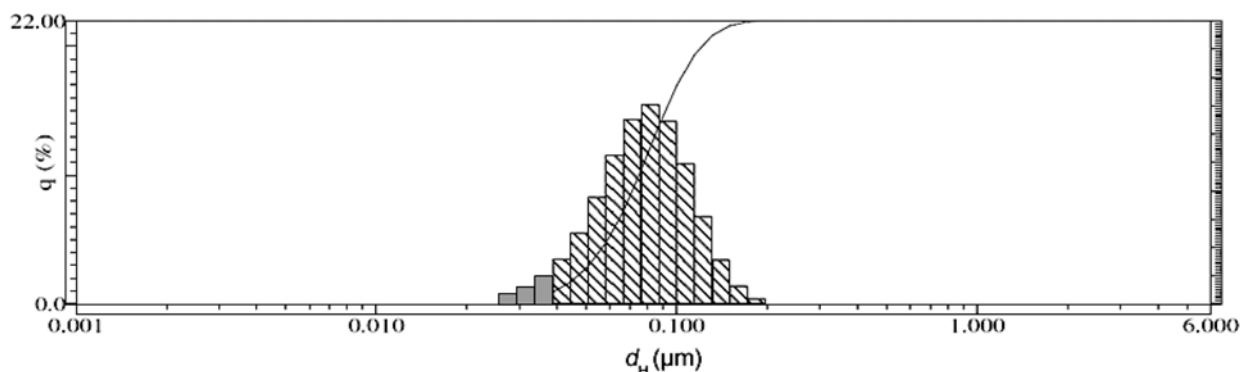


Fig. 5: The particle size distribution of the CM-dextran-coated maghemite nanoparticles in sample (B) measured using dynamic light scattering.

given. As such, V and K correspond to the individual particle properties, where K represents the anisotropy constant, k_B is the Boltzman constant and V is the particle volume.

The magnetization vs. the magnetic field of the as-synthesized and CM-dextran-covered maghemite particles are shown in Fig. 6b. The uncoated particles show no hysteresis, exhibiting a saturation magnetization of 65.2 emu/g. This value is smaller than that for the bulk materials $M_{\text{bulk}} = 88$ emu/g. The reduction of the magnetization of the magnetic particles with the decreasing particle size is usually caused by the incomplete coordination of the atoms on the particle surface, leading to a non-collinear spin configuration that causes the formation of a surface spin canting forming a nonmagnetic layer, i.e., a “dead layer”, which might reduce the particle’s magnetization.^{20,21}

We can estimate the thickness of this layer in sample (B) by applying the equation of Zheng et al.²²

$$M_{\text{sat}} = M_{\text{Bulk}}(1 - 6t/d) \quad (1)$$

where t is the thickness of the surface layer, d is the diameter of the particles, and M_{sat} and M_{Bulk} are the total sa-

turation of the whole particle and of its bulk, respectively. When M_{sat} is deduced from the experimentally determined saturation magnetization of 65.2 emu/g, M_{Bulk} is taken as the bulk value (88 emu/g) and $d_{\text{TEM}} = 14.5$ nm, as obtained from the TEM images of the as-prepared particles, we obtain a thickness for the “dead layer” of $t = 0.62$ nm.

The $M(H)$ dependence at 293 K of the samples (A) and (B) was analyzed by considering a log-normal particle size distribution, as described in,²³ and using a volumetric particle packing fraction $\varepsilon = 1$ for solid nanoparticles (non-magnetic fluid) in our case. We calculated the median diameter of the distribution $d_A = 8.20$ nm and the standard deviation $\sigma_A = 0.37$ for sample (A) and $d_B = 8.17$ nm and the standard deviation $\sigma_B = 0.36$ for sample (B).

Considering the estimated “dead layer” $2t = 1.24$ nm and the standard deviation we can compare this value with those obtained from the TEM images of the samples (A) and (B). Namely, the magnetic measurement “sees” only the magnetic phase, while that obtained from the TEM images also includes the so-called “dead layer”, which is not otherwise registered by the magnetic measurements.

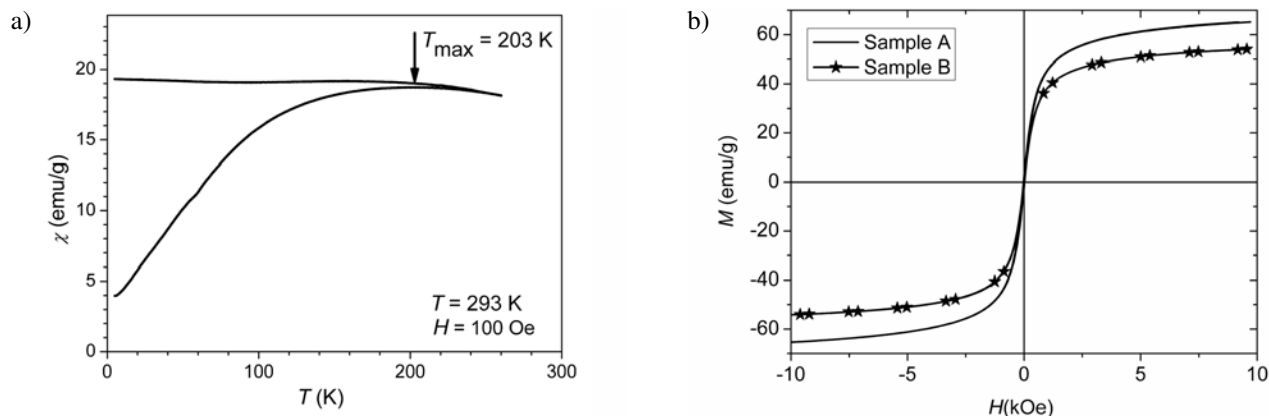


Fig. 6. a) ZFC and FC magnetization of coated maghemite particles (B) in the MF, $T_B = 203$ K, b) hysteresis of as-synthesized maghemite particles (A) and CM-dextran-coated particles (B) at 300K.

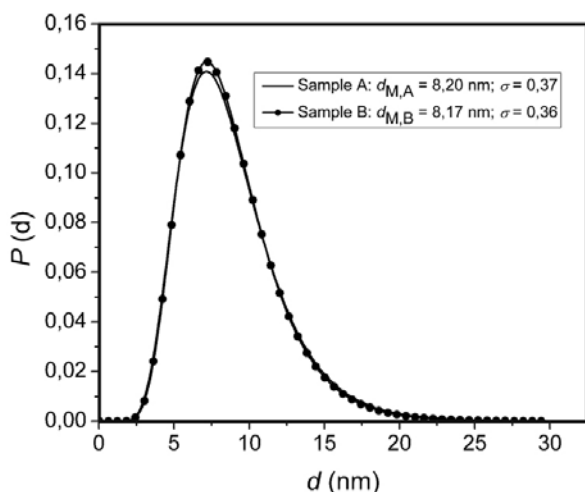


Fig. 7. Size distributions of sample (A) and sample (B), deduced from the fit of the magnetization curves.

The size distribution of the magnetic particles resembles that determined from the TEM images, albeit with a smaller average particle size. Average particles diameters for our particles determined using various experimental methods are collected in Table I.

Table 1. Average particle diameter of samples (A) and (B) obtained using different methods.

	d_{XRD} (nm)	d_{TEM} (nm)	d_{M} (nm)	d_{H} (nm)
Sample A	16.0	14.5	8.20	/
Sample B	11.8	12.0	8.17	77.9

3. 4. 1. Dissipation Mechanism

An AMF magnetic field will normally induce heating in a MF due to the dissipation of heat from the magnetic particles that is caused by the delay in the relaxation of the magnetic moment due to the Neel relaxation (which refers to the rotation of the magnetic moment within the particle) and the Brown relaxation (which refers to the rotation of the particle itself). The characteristic time for the Neel relaxation is:

$$\tau_{\text{N}} = \tau_0 \exp(KV/k_{\text{b}}T) \quad (2)$$

where k_{b} is the Boltzmann constant, T is the absolute temperature, τ_0 is the time constant $\approx 10^{-9}$ s, K is the anisotropy constant and V is the volume of the particle, while the Brown relaxation time is given by the relation:

$$\tau_{\text{B}} = 3\eta V_{\text{H}} / kT \quad (3)$$

where η is the viscosity of the carrier liquid, V_{H} is the

hydrodynamic volume of the particle, k_{b} is the Boltzmann constant, and T is the absolute temperature.

According to,²⁴ the volumetric power dissipation can be expressed as:

$$P = \pi\mu_0\chi''H_0^2f \quad (4)$$

where χ'' is the imaginary part of the complex AC susceptibility and is related to the material parameters of the magnetic fluid $\chi'' = \chi_0[\omega\tau/(1 + (\omega\tau)^2)]$, $\mu_0 = 4\pi \cdot 10^{-7}$ (Tm·A⁻¹) is the permeability of free space, τ is the effective relaxation time, and the overall relaxation time is given as $1/\tau = 1/\tau_{\text{N}} + 1/\tau_{\text{B}}$, where the shortest term governs the dominant mechanism and $f = \omega/2\pi$ is the frequency of the applied magnetic field. The above relaxations govern the dissipation of the magnetic energy, which then heats the magnetic fluid.

The morphology of the magnetic particles, their anisotropy constant and the carrier liquid's viscosity play a crucial role during the absorption of the magnetic energy when the magnetic fluid is subjected to an AMF magnetic field. All the parameters are implicitly involved in the effective relaxation time τ . The theoretical estimation of the SAR as a function of the particle diameters and the magnetic field at 104 kHz calculated using the equations above is in Fig. 8.

The theoretical estimation of the SAR at room temperature as a function of the monodispersed particle size shows a maximum that increases with frequency and is centered on a particle size around 15.3 nm. In Table I the average particle diameter for our particles in sample (B) determined using various experimental methods is between 8 and 12 nm. The pronounced dependence of SAR on the particle diameter is mostly related to the Neel relaxation. Here, the Neel relaxation time depends exponentially on the magnetic anisotropy and the particle volume, while the Brownian time depends linearly on the particle volume/size and the solvent viscosity.

3. 4. 2. SAR Measurements

The specific absorption rate (SAR) of the sample was measured calorimetrically in an AMF with a frequency of 104 kHz and a magnetic field amplitude ranging from 1.5 to 3.0 kA/m, which is in the range of biomedical applications for magnetic hyperthermia.²⁶

From the course of the temperature increase, Fig. 9, the SAR was estimated as:

$$\text{SAR} = (C_{\text{solvent}} / x_{\text{iron oxide}}) (\Delta T/\Delta t) \quad (5)$$

where C_{solvent} is the heat capacity of the solvent ($C = 4.18$ J K⁻¹g⁻¹ for water), $x_{\text{iron oxide}}$ is the weight fraction of iron oxide and $(\Delta T/\Delta t)$ is the initial slope of the time dependence of the self-heating temperature.

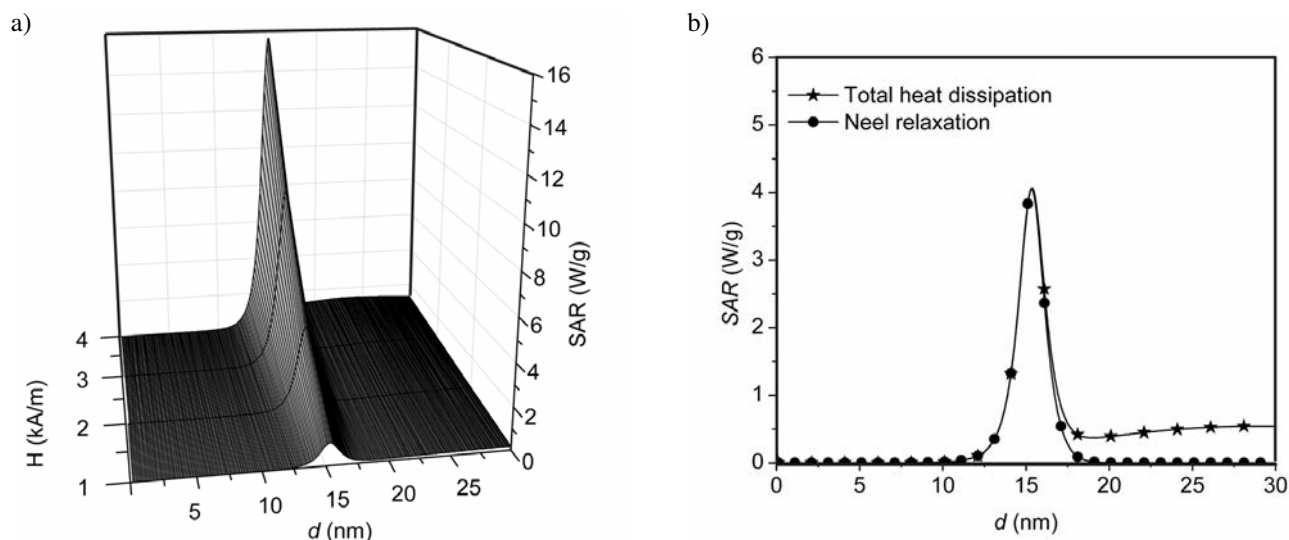


Fig. 8. a) Theoretical estimation of the SAR at room temperature as a function of the particle diameter (d) and the AMF magnetic field (H). Here we have K (anisotropy constant) = 16 kJ/m^3 ,⁶ $T = 293 \text{ K}$, $\eta = 1\text{E-}03 \text{ Pas}$ (viscosity of the media – of water), $f = 104 \text{ kHz}$ and CM-dextran layer thickness $\delta = 18 \text{ nm}$ (calculate as L_{min}^{25}) and b) total heat dissipation through Neel and Brownian relaxation at $f = 104 \text{ kHz}$ and $H = 2 \text{ kA/m}$ (difference between total heat dissipation and Neel relaxation losses is the Brownian relaxation losses).

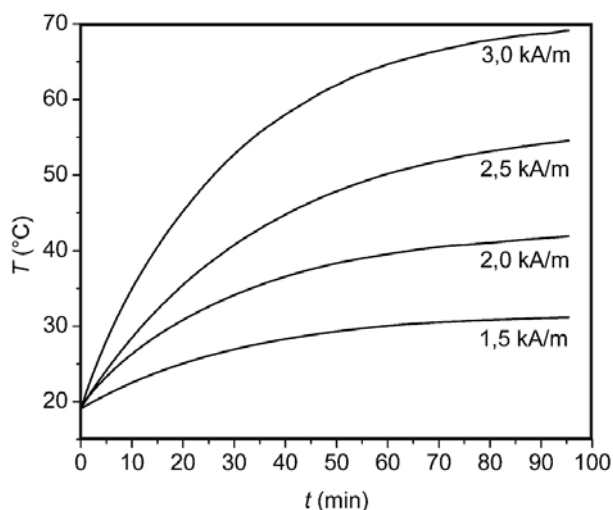


Fig. 9. Time dependence of the self-heating temperature on the magnetic field at 104 kHz for sample (B).

After a certain period of self-heating the steady state was achieved when the generated heat at constant temperature was equal to that lost to the environment due to thermal convection. The maximum temperature of this steady state is important when using iron-oxide-based MFs with a high Curie temperature for “in vivo” applications, because this is the only way to use such a MF without damaging the surrounding tissue during the magnetic hyperthermia. In Fig. 10, the temperature of the magnetic fluid at the steady state is plotted vs. the applied magnetic field.

In the system considered the steady state at, e.g., $42.^\circ\text{C}$, is achieved at 2.0 kA/m (104 kHz). These condi-

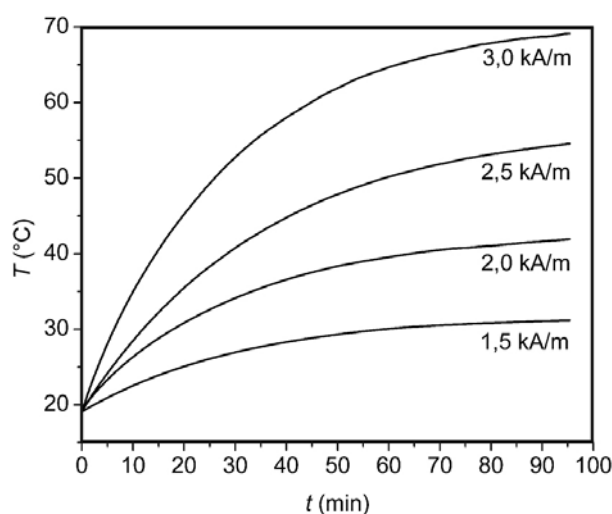


Fig. 10. Temperature of the system of the magnetic fluid in the calorimeter at steady state vs. the applied magnetic field at a constant frequency ($f = 104 \text{ kHz}$).

tions can be achieved reproducibly and might serve as a guarantee that in a situation when instead of the system being considered a human tissue is considered and/or an “in vivo” application, the overheating of the tissue can be completely avoided. The SAR needed to heat the system to the desired temperature, for these samples at 42°C was $\text{SAR}_{104 \text{ kHz}, 2.0 \text{ kA/m}} = 0.854 \text{ W/g}_{\text{iron oxide}}$. Some typical SAR data for a MF based on water as a carrying liquid and iron oxide (maghemite) as the magnetic phase are shown in Table II.

The theoretical estimation of the SAR shows that the main relaxation mechanism is due to the Neel relaxation, while the Brown relaxation is small and its contribution to

Table 2. Some typical SAR data for a MF based on maghemite particles.

d (nm)	H (A/m)	f (kHz)	SAR (W/g)	SAR normalized*	References
8	24800	700	37	0.036	6
10.2	24800	700	275	0.266	6
12	2000	104	0.854	0.854	our
15.3	11000	410	600	5.030	27
16/12.8	27000	700	952	0.776	28

* normalized to $H = 2.0$ kA/m and $f = 104$ kHz

the dissipation mechanism must be very limited, Fig. 8. a, b. This can be substantiated by the DLS spectra. The smallest particle diameter d_H that would ensure a relaxation time which would follow the fast changes of the magnetic fields at 104 kHz and contribute to the Brown relaxation must show a relaxation time of $\tau_b \leq 10^{-5}$ s, thus exhibiting a particle size of $d_H \leq 29.5$ nm, estimated using equation (2). All the other particles with a larger hydrodynamic diameter, i.e., agglomerates, will be not active in the heating of the MF in a high-frequency magnetic field (HFMF).

Thus, based on the consideration above, only a very small fraction of the composite particles in sample (B) are able to contribute to the Brown relaxation. All the others are agglomerated in clusters and cannot rotate and the heating contribution of the Brown relaxation can be excluded from the total magnetic dissipation.

To reveal the mechanism that governs the major losses in sample (B), samples with immobilized particles were also prepared. The particles of the original magnetic fluid were immobilized by a drastic increase of the viscosity. The magnetic particles were dispersed in an aqueous solution of gelatin (sol).²⁹ An abrupt increase in the visco-

sity, by many orders of magnitude, can be achieved, and consequently viscous losses can be eliminated by simply freezing the Brownian motion of the magnetic particles.

In Fig. 11 the time dependence of the self-heating temperature on the magnetic field at 104 kHz for testing the magnetic fluid with agar and without it is shown.

It can be seen that the increase of the self-heating temperature of MF of sample (B) is a little higher than that of the MF(agar) sample where the Brown relaxation is not possible, Fig. 11. We believe that this small difference in the SAR is caused due to the Brown relaxation of particles in the sample (B) where a very small fraction of single particles with a hydrodynamic radii $d_H \leq 29.5$ nm, Fig. 5, can freely rotate and contribute to the Brown relaxation. One can calculate approximately its separate contribution from the SAR difference at the steady state for both samples using the corresponding $(\Delta T/\Delta t)_{\text{steady state}}$ for both curves and eq. (4). This estimated contribution is alike to that obtained directly from the diagram on the Fig. 11 at the steady state. The Brown contribution was confirmed to be about 5%.

4. Conclusions

Our results have shown that the high Curie point of a magnetic particle, which can damage the tissue during a magnetic hyperthermia treatment, can be circumvented by applying a controlled particle morphology. The heat flow is adjusted with the AMF magnetic field intensity and/or frequency so that the generated heat at the selected temperature and location will be equal to that lost to the environment due to heat exchange. Furthermore, the investigation revealed that the major heat dissipation in our sample (B) came from the Neel relaxation losses. Here, the particle size governs the extent of the Neel relaxation process, while the Brown-based dissipation is very small. Here, the number of the particles with a suitable r_H which absorb in the Brownian relaxation range is very small and contribute only 5% to the total SAR.

6. Acknowledgements

This work was supported by the Ministry of Education, Science and Sport of Slovenia. The authors also wish to acknowledge Miloš Beković for his help in SAR measurements.

7. References

1. A. E. Merbach, E. Toth: The chemistry of contrast agents in medical magnetic resonance imaging, John Wiley & Sons, Chichester, England, 2001.
2. T. Neuberger, B. Schöpf, H. Hofmann, M. Hofmann, B. Rechenberg, *J. Magn. Magn. Mater.* 2005, 293, 483–496.

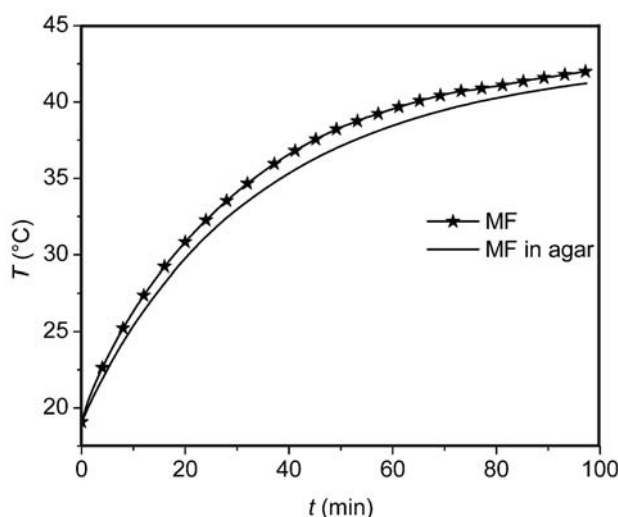


Fig. 11. Dependence of the self-heating temperature on time at a magnetic field frequency of 104 kHz and a magnetic field amplitude of 2.0 kA/m for a magnetic fluid with agar and without it.

3. A. Ito, M. Shinkai, H. Honda, T. Kobayashi, *J. Biosci. Bioeng.* **2005**, *100*, 1–11.
4. U. Häfeli, W. Schütt, J. Teller, M. Zborowski (Eds.), *Scientific and Clinical applications of Magnetic Carriers*, Plenum Press, New York, **1997**, 569–595.
5. A. K. Gupta, M. Gupta, *Biomaterials* **2005**, *26*, 3995–4021.
6. J. P. Fortin, C. Wilhelm, J. Servais, C. Menager, J. C. Bacri, F. Gazeau, *J. Am. Chem. Soc.* **2007**, *129*, 2628–2635.
7. A. Skumiel, M. Labowski, H. Gojzewski, *Mol. Quant. Acoust.* **2007**, *28*, 229–239.
8. D. Kirpotin, D. C. F. Chan, P. A. Bunn, Magnetic microparticles, US Patent Number 5,411,730, date of patent May 2, **1995**.
9. J. Lee, T. Isobe, M. Senna, *J. Colloid Interface Sci.* **1996**, *177*, 490–494.
10. M. Suzuki, M. Shinkai, M. Kamihira, T. Kobayashi, *Biotechnol. Appl. Biochem.* **1995**, *21*, 335–345.
11. V. Veiga, D. H. Ryan, E. Sourty, F. Llanes, R. H. Marchessault, *Carbohydr. Polym.* **2000**, *42*, 353–357.
12. K. Donadel, M. D. V. Felisberto, V. T. Fávere, M. Rigoni, N. J. Batistela, M. C. M. Laranjeira, *Mater. Sci. Eng., C* **2008**, *28*, 509–514.
13. S. Dutz, W. Andrä, R. Hergt, R. Müller, C. Oestreich, C. Schmidt, J. Töpfer, M. Zeisberger, M. E. Bellemann, *J. Magn. Magn. Mater.* **2007**, *311*, 51–54.
14. M. Bekovic, I. Ban, A. Hamler, Assessment of magnetic fluid losses out of magnetic properties measurement, *J. Phys.: Conf. Ser.* **2010**, *200*, 1–4.
15. A. Carpov, G. G. Bumbu, G. C. Chitanu, C. Vasile, *Cellul. Chem. Technol.* **2000**, *34*, 455–471.
16. X. Q. Xu, H. Shen, J. R. Xu, J. Xu, X. J. Li, X. M. Xiong, *Appl. Surf. Sci.* **2005**, *252*, 494–500.
17. M. P. Morales, S. Veintemillas-Verdaguer, M. I. Montero, C. J. Serna, *Chem. Mater.* **1999**, *11*, 3058–3064.
18. M. Ibrahim, A. Nada, D. E. Kamal, *Indian J. Pure Appl. Phys.* **2005**, *43*, 911–917.
19. Y. T. Tao, *J. Am. Chem. Soc.* **1993**, *115*, 4350–4358.
20. J. M. D. Coey, *Phys. Rev. Lett.* **1971**, *27*, 1140–1142.
21. R. H. Kodama, A. E. Berkowitz, E. J. McNiff, S. Foner, *Phys. Rev. Lett.* **1996**, *77*, 394–397.
22. M. Zheng, X. C. Wu, B. S. Zou, Y. J. Wang, *J. Magn. Magn. Mater.* **1998**, *183*, 152–156.
23. R. W. Chantrell, J. Poplewell, S. W. Charles, *IEEE Trans. Magn.* **1978**, *14*, 975–977.
24. R. E. Rosensweig, *J. Magn. Magn. Mater.* **2002**, *252*, 370–374.
25. T. Kawaguchi, M. Hasegawa, *J. Mater. Sci.: Mater. Med.* **2000**, *11*, 31–35.
26. A. Jordan, R. Scholz, P. Wust, H. Fähling, R. Felix, *J. Magn. Magn. Mater.* **1999**, *201*, 413–419.
27. R. Hergt, R. Hiergeist, I. Hilger, W. A. Kaiser, Y. Lapatnikov, S. Margel, U. Richter, *J. Magn. Magn. Mater.* **2004**, *270*, 345–357.
28. M. Lévy, C. Wilhelm, J. M. Siaugue, O. Horner, J. C. Bacri, F. Gazeau, *J. Phys.: Condens. Matter* **2008**, *20*, 204133.
29. R. Hergt, R. Hiergeist, M. Zeisberger, G. Glöckl, W. Weitschies, L. P. Ramirez, I. Hilger, W. A. Kaiser, *J. Magn. Magn. Mater.* **2004**, *280*, 358–368.

Povzetek

V prispevku je predstavljena sinteza in karakterizacija magnetnih maghemitnih nanodelcev prevlečenih s karboksimetil dekstranom (CM-dekstran), primernih za uporabo v magnetni hipertermiji. Stopnjo specifične absorpcije (SAR) stabilne magnetne tekočine pripravljene iz maghemitnih nanodelcev prevlečenih s CM-dekstranom, smo preverili s pomočjo kalorimetričnih meritev magnetne tekočine izpostavljene zunanjemu izmeničnemu magnetnem polju. Rezultati kažejo, da velikost magnetnih nanodelcev in debelina prevleke CM-dekstrana vplivata na stopnjo specifične absorpcije (SAR), pri čemer večji del toplotnih izgub izhaja iz Neel-ove relaksacije, medtem ko je prispevek Brown-ove relaksacije majhen. Termično ravnotežje pri ciljni temperaturi (42 °C) lahko dosežemo s primernimi morfološki lastnostmi sintetiziranih magnetnih nanodelcev maghemita in s kontroliranjem jakosti ali frekvence zunanjega izmeničnega magnetnega polja.